INTERNATIONAL JOURNAL OF
COASTAL, OFFSHORE & ENVIRONMENTAL ENGINEERING IJCOE Vol.7/No. 3/Summer 2022 (20-30)

Available online at: www. Ijcoe.org

Assessment of long-term consistency of ocean-color satellite-derived chlorophyll-a products in the Persian Gulf

Masoud Moradi[1*,2]

*[*1] Iranian National Institute of Oceanography and Atmospheric Science (INIOAS); Moradi_msd@yahoo.com*
[2] Center for International Scientific Studies & Collaboration (CISSC), ministry of Science Research and Technology, Tehran, Iran

ARTICLE INFO

Article History:
Received: 07 Dec. 2021
Accepted: 16 Aug. 2022

Keywords:
Remote sensing
Ocean color
Atmospheric correction
Coastal waters
Correlation analysis

ABSTRACT

Over the past two decades, several ocean color satellites have operated in parallel. The combination of different ocean color satellite sensor products is a vital task for studying the biogeochemistry of seas. In this study, we evaluated the temporal consistency of the monthly time-series and monthly interannual variations of satellite-derived chlorophyll-a concentrations (Chl-*a*) from four satellite sensors during 2002-2020 period over the Persian Gulf. Statistical correlation between Chl-*a* time series and anomalies from selected satellite sensors were significantly correlated for 84% area of the Persian Gulf. Correlations were reasonably sensitive to the choice of Chl-*a* retrieval and atmospheric correction algorithms. The standard algorithms for Chl-*a* retrieval showed the lowest value of correlations, and it was indicated that these algorithms were not suitable for Chl-*a* estimations from satellite sensors over the Persian Gulf. The OCI algorithm for Chl-*a* retrieval showed more consistency among different satellite sensors and it was shown that it is more suitable than previous ones for estimation of Chl-a from selected satellite sensors. Also, it was shown that the SeaDAS and POLYMER atmospheric correction algorithms have a great influence on the Chl-*a* estimations from selected satellite sensors. It was shown that more than 70% of the study area indicated imperfect consistency between selected atmospheric correction algorithms applied on different satellite sensors. Choosing the best atmospheric correction and Chl-*a* retrieval algorithms is the most important task in the estimation and utilization of Chl-a in the Persian Gulf.

1. Introduction

Phytoplankton biomass is a crucial indicator of ocean biology, and it has been used to predict climate change and the state of the oceans [1–3]. Understanding of ocean biology and marine ecosystems, and as well as their interactions, would be achieved by knowledge of spatial and temporal variations of phytoplankton biomass [4–6]. Long-term and interannual variations phytoplankton biomass and primary productivity and of the marine ecosystem are economically important in fisheries and marine resource management [7,8]. The near-surface chlorophyll-a concentration derived from ocean color sensors (Chl-*a*) is the most valuable factor to study the phytoplankton biomass [9].

Various ocean color satellite sensors have produced useful long-term data collections over the ocean's surface layer for the past three decades [7,10,11]. Remote sensing of ocean color is expected to be the primary source of data for detecting long-term changes in phytoplankton biomass due to the spatial and temporal sampling capabilities of corresponding satellite data [12]. However, the lifespans recent satellites (5-10 years) are insufficient to analyze the response of phytoplankton biomass to climate change and the other long-term climatological and environmental indicators [13]. In this regard, combination of different satellite sensor datasets is an ideal approach to study the changes in phytoplankton biomass and the effect of climate and environmental factors on their variabilities [3,12]. During the past three decades, many ocean color satellites have been lunched to study the biological characteristics of the oceans and marine environments. Among them, Sea-viewing Wide Field-of-view Sensor (SeaWiFS) (1997-2010), Moderate Resolution Imaging Spectrometer (MODIS) (2002-present), Medium Resolution Imaging Spectrometer (MERIS) (2002-2012), and Visible Imager Radiometer (VIIRS) (2011-present) have been used extensively in biological oceanography.

Several researches have tried to evaluate the variability and seasonal cycles of Chl-*a* estimated from two or more ocean-color satellite sensors [14–16]. However, there are limited documents on the consistency of seasonal and interannual variations of Chl-*a* among SeaWiFS, MERIS, MODIS, and VIIRS in a long-period (e.g. >10 years). Furthermore, the sensitivity of the different Chl-*a* retrieval algorithms and atmospheric-correction have not been considered in the assessment of multi merged ocean color satellite sensors applications. consequently, temporal consistency of correlation between Chl-*a* products from different satellite sensors remains a challenging issue.

In this paper, we demonstrate the seasonal and interannual fluctuations in monthly Chl-*a* products for SeaWiFS, MERIS, MODIS, and VIIRS over the Persian Gulf using statistical methods.

2. Data and Methods

2.1. Study area

Persian Gulf is a shallow marginal sea which connects to the Gulf of Oman through the Strait of Hormuz. Persian Gulf is dominantly shallow with average depth of 30 m and maximum depth of ~90 m [17]. The surrounding areas are hot and dry during March-October, and precipitation rate is very low (<300 mm y^{-1}) [18]. Persian Gulf is surrounded by deserts where are the source of frequent dust storms. The number of observed dust storms reach 15-20 per year and usually caused by winds blowing from Arabian Sea (*Shamal* wind) and north-east Africa [19]. Surface currents enters the Gulf from Strait of Hormuz and then reverse back along the southern coasts [20,21].

Many researchers have used ocean color data to study the spatial-temporal variations and dynamics of phytoplankton in the Persian Gulf [16,22–24]. Phytoplankton growth is highly influenced by dust deposition and fertilization in the Persian Gulf which leads to monstrous growth and generation of algal blooms [23,25,26]. Oceanographic and atmospheric factors are the main parameters that control the variability of Chl-*a* in this area. Consequently, the effect of these factors on optical properties of atmosphere and Chl-*a* retrieval algorithms increase the uncertainties in the satellite-derived Chl-*a* concentrations. To date, several studies aimed to evaluate the effect of atmosphere on Chl-*a* accuracy in the southern parts of the Persian Gulf [15,27]. However, the accuracy of Chl-*a* retrieval algorithms and also consistency of long-term Chl-*a* series from different satellite sensors have not been determined. To evaluate the effect of uncertainties on the Chl-*a* retrieval algorithms, we have to compare the available Chl-*a* products and determine how they are comparable, and how they are affected by atmospheric and retrieval algorithms.

2.2. Satellite data

The monthly level-3 Standard Mapped Imageries of SeaWiFS, MERIS, MODIS, and VIIRS Chl-*a* datasets with spatial resolution 4km×4km were downloaded from NASA ocean-color website (http://oceancolor.gsfc.nasa.gov/) for the time period 2002-2020. The selected datasets have been processed using a conceptually similar atmospheric correction algorithm [3,28] and Chl-*a* retrieval algorithms [29,30]. The performed atmospheric correction is considered as a common framework that removes the bad data influenced by high sensor view angle, high solar-zenith angels, high aerosol loads, sun glint and stray-light contamination. The Chl-*a* retrieval algorithms estimate the chlorophyll-*a* concentrations using empirical blue-green reflectance band ratio, and tune the specific wavelengths of each sensor. We used monthly datasets because: (i) they are usually the smallest time frame during which the highest spatial coverage for a single sensor may be achieved (>80%) [31], (ii) the results of this study may be comparable with previous studies that use long-term analysis [9,32,33], (iii) unwanted satellite sensor noises are filtered in the monthly averaged time-series data, and (iv) it reduces the analysis computing time.

In addition to the above standard Chl-*a* products, other Chla- datasets have been downloaded and processed during the same period and similar spatial properties from the NASA ocean-color website to evaluate the consistency of Chl-a time-series on a single sensor, and among the selected four sensors. This help us to select the best Chl-*a* dataset from each single sensor and decide how different atmospheric correction and Chl-*a* retrieval algorithms influence the products. The GSM or OCI bio-optical algorithms have been used to process these additional Chl-*a* products. The GSM algorithm considers the absorption by combined detrital and dissolved matter and particle backscattering to retrieve Chl-*a* using a semi-analytical inversion model [34,35]. The OCI performs a band-difference of remote-sensing reflectance in the green part of the visible spectrum, and tunes the results using a linear baseline between blue and red wavebands [30,36]. This algorithm is applicable only in oligotrophic waters where Chl-*a*<0.25 mg m^{-3} and reverts to standard band-ratio algorithm at higher Chl-*a*>0.3 mg m^{-3}.

In addition to the standard MERIS data, additional MERIS datasets were processed using a different atmospheric correction algorithm called POLYMER to evaluate the sensitivity of Chl-*a* time-series to the variations of atmospheric correction algorithms. The standard Chl-*a* products have been processed using SeaDAS atmospheric correction algorithm. In contrast,

Table 1- List of satellite datasets used in this study. The acronyms in the last column indicate the performed atmospheric correction and chlorophyll-a retrieval algorithms, and are used as reference to the selected corresponding dataset.

Sensor	Atmospheric correction	Chl-*a* retrieval	Duration	Acronym	
SeaWiFS	SeaDAS	OC4	1997-2010	SeaWiFS-SO	*Comparison-I*
MERIS	SeaDAS	OC4E	2002-2012	MERIS-SO	
MODIS	SeaDAS	OC3M	2002-present	MODIS-SO	
VIIRS	SeaDAS	OC3V	2012-present	VIIRS-SO	
MODIS	SeaDAS	OC3M	2002-present	MODIS-SO	*Comparison-II*
MODIS	SeaDAS	GSM	2002-present	MODIS-SG	
MODIS	SeaDAS	OCI	2002-present	MODIS-SI	
MERIS	SeaDAS	OC4E	2002-2012	MERIS-SO	*Comparison-III*
MODIS	SeaDAS	GSM	2002-present	MODIS-SG	
SeaWiFS	SeaDAS	OCI	1997-2010	SeaWiFS-SI	
MERIS	POLYMER	OC4E	2002-2012	MERIS-PO	*Comparison-IV*
SeaWiFS	SeaDAS	OC4	1997-2010	SeaWiFS-SO	
MODIS	SeaDAS	OC3M	2002-present	MODIS-SO	
MERIS	SeaDAS	OC4E	2002-2012	MERIS-SO	

POLYMER algorithm is a coupled ocean-atmosphere algorithm based on spectral optimization, and it conceptually differs with SeaDAS [9]. The POLYMER algorithm for MERIS sensor shows a more ability to perform in the presence of sun glint, and therefore it generates extensible spatial coverage that did not observe in the other atmospheric correction algorithms [3].

The list of selected Chl-*a* datasets and corresponding atmospheric correction and Chl-*a* retrieval algorithms are show in Table 1. Here, the following four comparisons were made:

- *Comparison-I*: Chl-*a* datasets of SeaWiFS-SO, MERIS-SO, MODIS-SO, and VIIRS-SO were used to compare their temporal consistency during the study period using a common framework.
- *Comparison-II*: Chl-*a* datasets of MODIS-SO, MODIS-SG, and MODIS-SI were used to assess the impacts of different Chl-*a* retrieval algorithms on the temporal comparisons of a single sensor.
- *Comparison-III*: Chl-*a* datasets of MERIS-SO, MODIS-SG, and SeaWiFS-SI were used to assess the impacts of different Chl-*a* retrieval algorithms on the temporal consistency of different sensors.
- *Comparison-IV*: Chl-*a* datasets of SeaWiFS-SO, MODIS-SO, MERIS-SO, and MERIS-PO were used to assess the impacts of different atmospheric correction algorithms on the temporal consistency of Chl-*a* time-series.

In general, Chl-*a* datasets are log-normally distributed over the coastal areas and marginal seas [37]. Hence, all Chl-*a* imageries were transformed in Log_{10} bases prior to further analysis.

2.3. Calculate monthly climatology and anomaly

Monthly climatologies of the selected datasets were produced at each grid pixel. The Chl-*a* monthly climatology products of each satellite sensors were calculated for the whole period using Climate Data Toolbox for MATLAB® [38]. To calculate the monthly climatologies, the same number of observations and a common grid point were used for each of the selected Chl-*a* product to compute the monthly climatology. As a result, any biases and errors caused by missing data were consistent among different Chl-*a* products, and therefore the minimal effect of missing data was achieved. In addition, monthly anomalies were calculated for further analysis. Monthly anomalies were calculated by subtracting the monthly climatology from the corresponding monthly time-series datasets of each grid point for selected sensors during the study period. After that, the monthly Chl-*a* time-series and anomalies were transformed in Log10 bases (here after will be shown as Log10(Chl-*a*)) to fully cover the log-normal distribution of these datasets.

2.3. Statistical analysis

The Pearson correlation coefficient (r), as the most known index for correlation of variables, was used in this study. Pearson correlation coefficient assumes that the variables are normally distributed and a linear relationship exists between them. Based on the probability of the correlation between variables, the significance of each correlation (p) was calculated.

The linear regression type-1 was selected to calculate the trend of Chl-*a* datasets of each satellite sensor product. The type-1 linear regression was selected because: (a) it has been widely used for detection of

Chl-*a* trends [39], (b) comparison of log-transformed Chl-*a* anomalies and time-series are well recognized than those observed by complex trend detection methods [3], and (c) we are going to test whether trends between different sensor products provide an insight to the correlation between them, and we do not looking for the exact trends in the datasets. Trends in Chl-*a* time-series and anomalies data is computed as:

$$Y = XS + I \quad (1)$$

where 'Y' is the log-transformed anomaly, 'X' is time in year, 'S' is the slope of regression, and 'I' is the intercept. In this equation, 'S' defines the trend, and it is shown only when the Pearson correlation coefficient (r) was statistically significant ($p<0.05$).

In this study, we used the Z-test to identify whether two correlation coefficients are statistically different [40]. The score of a known r-value for two separate correlations is determined as bellow:

$$Z_n = 0.5log\left(\frac{1+r_n}{1-r_n}\right) \quad (2)$$

where Z_n is the score of each r-value. The overall Z_{score} is computed as bellow (Cohen and Cohen, 1983):

$$Z_{score} = \frac{Z_n - Z_{n+1}}{\{[1/(m_n-3)] + [1/(m_{n+1}-3)]\}^{1/2}} \quad (3)$$

where Z_{score} is then converted into the p-value assuming normal distribution of target datasets. A two-tailed test was performed to estimate accurate p-values. If $p<0.05$ the r-values are considered to be statistically significant and different, otherwise they deemed to be similar.

3. Results

3.1. Comparison of the standard Chl-a products (Comparison-I)

Correlation coefficient (r) between standard monthly Chl-*a* time-series from different satellite sensors are shown in Fig. 1. Over the most of the study area, the Chl-a time-series of the different satellite sensors show a high correlation (>0.85). The significance of correlations between different satellite sensors shows that the correlation between MODIS-SO and VIIRS-SO differs from the other pairs. Correlation between pairs of the Comparison-I, except the MODIS-SO vs. VIIRS-So, show that the 49-64% of the study area are very highly correlated ($p<0.0001$), 76-83% are highly correlated ($p<0.01$), 84-89% are significantly correlated ($p<0.05$), and 11-15% are not significant (Fig. 1 e-f) (Table 2). Correlation between MODIS-SO and VIIRS-SO shows that the only 9% of the study area are very highly correlated, 24% are highly correlated, 37% are significantly correlated, and 63% are not significantly correlated (Fig. 2h). The most important reason for this observation rises from the missing data over the study area between MODIS-SO and VIIRS-SO during the 2012-2020. The significantly correlated areas ($p<0.05$) are remarkably similar and the middle parts of the Persian Gulf show greatest r-values relative to the shallow regions. It is suggested that the shallow regions are affected by noises when compared with deeper regions.

Fig. 2a-d shows the r-values between monthly Chl-*a* anomalies from different ocean color sensors. The anomalies of Chl-*a* time-series represent the removed seasonal cycles from original data. After removing the seasonal cycles from Chl-*a* time-series, the correlations between sensors are not as high as the time-series in Fig. 1. It has been shown that the main fluctuation of Chl-*a* in the Persian Gulf is due to seasonal cycles. Hence, the large part of the total variance of Chl-*a* time-series is expected to be due to the seasonality, and the Chl-a anomalies reveal the interannual fluctuations of Chl-*a*. Nonetheless, over the most regions of the study area, Chl-*a* anomalies between different satellite sensors are highly correlated (>0.85), except the correlation between MODIS-SO vs. VIIRS-SO that shows r-values of 64-76%. The statistical significance of these correlations are considerably lower than those observed in Fig. 1e-h, with 63-69% of the total study area having significant correlation ($p<0.05$). Correlation between MODIS-SO and VIIRS-SO shows the lowest very high significant (4%), and about 65% percent of this correlation is insignificant (Table 2).

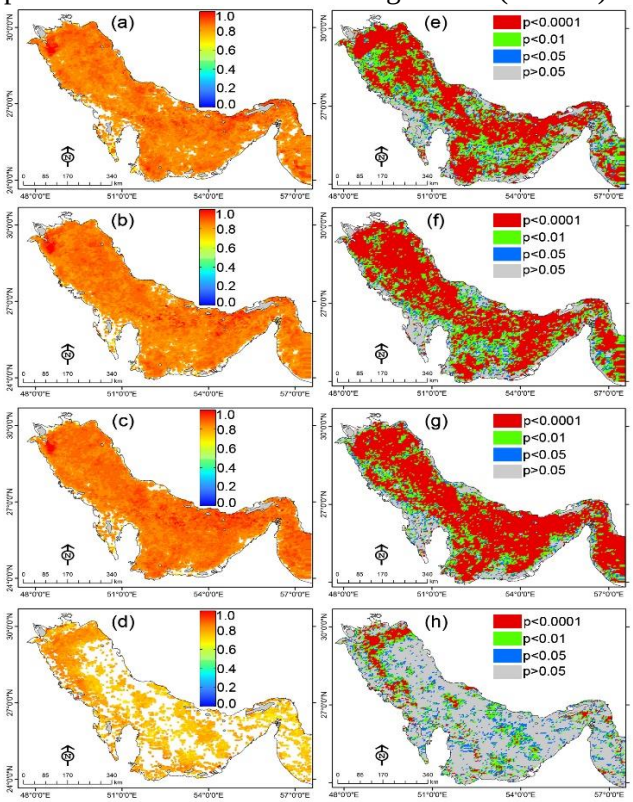

Figure 1. Maps of the correlation coefficient (r) between the monthly Chl-a time-series from different satellite sensors, Comparison-I. (a) MODIS-SO vs. MERIS-SO, (b) MODIS-SO vs. SeaWiFS-SO, (c) SeaWiFS-SO vs. MERIS-SO, (d) MODIS-SO vs. VIIRS-SO. (e)-(h) maps show the statistical significance (p) of the correlations of (a)-(d), respectively.

Table 2- Percentage area of the study area with significant (p<0.05), and not significant (p>0.05) correlations of the different comparisons denoted in table 1.

	Comparison	Chl-*a* time-series				Chl-*a* anomalies			
		p<0.0001	p<0.01	p<0.05	p≥0.05	p<0.0001	p<0.01	p<0.05	p≥0.05
I	MODIS-SO & MERIS-SO	49	76	84	15	24	49	63	37
	MODIS-SO & SeaWiFS-SO	57	81	87	12	25	52	66	34
	MERIS-SO & SeaWiFS-SO	64	83	89	11	26	55	69	30
	MODIS-SO & VIIRRS-SO	09	24	37	63	04	17	34	65
II	MODOS-SG & MODIS-SI	37	52	61	40	27	40	50	49
	MODIS-SG & MODIS-SO	12	25	34	65	06	16	25	75
	MODIS-SO & MODIS-SI	20	46	61	39	06	17	27	73
III	MERIS-SO & MODIS-SG	06	16	25	75	04	09	16	84
	MERIS-SO & SeaWiFS-SI	60	81	88	12	31	53	67	33
	MODIS-SG & SeaWiFS-SI	07	18	27	73	05	12	20	80
IV	MODIS-SO & MERIS-PO	04	12	21	79	03	07	13	87
	SeaWiFS-SO & MERIS-PO	06	13	22	77	05	11	18	82
	MERIS-SO & MERIS-PO	06	16	26	74	05	12	21	79

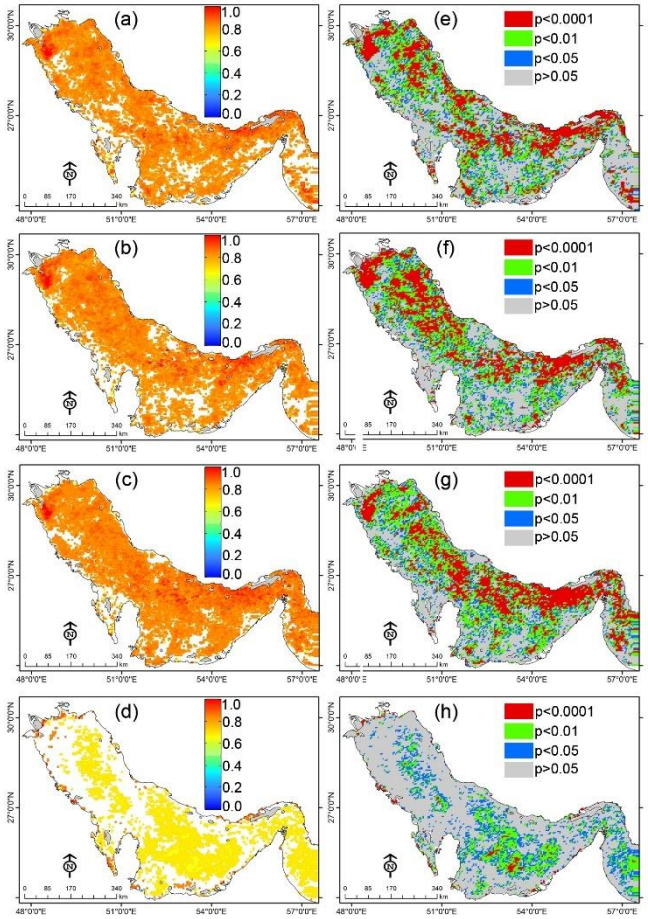

Figure 2- Maps of the correlation coefficient (r) between the monthly Chl-a anomalies from different satellite sensors, Comparison-I. (a) MODIS-SO vs. MERIS-SO, (b) MODIS-SO vs. SeaWiFS-SO, (c) SeaWiFS-SO vs. MERIS-SO, (d) MODIS-SO vs. VIIRS-SO. (e)-(h) maps show the statistical significance (p) of the correlations of (a)-(d), respectively.

3.2. Comparison of different Chl-a retrieval algorithms from a single sensor (Comparison-II)

Fig. 3 shows the correlation coefficient (r) and statistical significance (p) between Chl-*a* time-series from different Chl-*a* retrieval algorithms of MODIS. Results revealed that the Chl-*a* time-series are well correlated (>0.78) between different retrieval algorithms, but the most areas show the imperfect significant correlations (Table 2). The correlation between MODIS-SG and MODIS-SO shows the lowest significant values and less than 12% of the study area are very well correlated, and about 65% are not significantly correlated. The imperfect correlations are seen in the central parts and deeper regions where lower values of Chl-*a* are observed. Further, there are lower correlation (>0.70) in the Chl-*a* anomalies between different MODID data (Fig. 4). The Chl-*a* anomalies show the lowest correlation (~0.7) between MODIS-SO and MODIS-SI in the central parts of the Persian Gulf (Fig. 4c). The Chl-*a* anomalies show more correlations between different MODIS products in the shallow areas where p-values are significant. Despite the high correlation values of different Chl-*a* anomalies (>0.7) in the shallow areas of the study area, the majority of areas of the Persian Gulf do not show a significant correlation (p≥0.05) (Fig. 4d-f). This is mainly due to the gap of data between different Chl-*a* retrieval algorithms from MODIS data. Correlation coefficient (r-value) and probability maps (p-value) between monthly Chl-*a* time-series and anomalies from MODIS (Fig. 3a, c and 4a, c) revealed that the MODIS-SG vs. MODIS-SI shows the highest and the most significant correlation relative to the other sensor pairs proposed for Comparison-II. The worst case of comparison between Chl-*a* anomalies in Comparison-II belongs to the MODIS-SG vs. MODIS-SO pairs. Consequently, original time-series and removed seasonal cycles of Chl-*a* datasets using GSM and OCI retrieval algorithms agree perfectly in shallow high Chl-*a* waters (Fig. 4a) as OCI algorithm reverts to GSM algorithm at Chl-*a* concentrations >0.3 mg m^{-3}. In contrast, OC3M algorithm (MODIS-SO) shows the lowest agreement with SGM algorithm in both shallow and deeper areas, which indicates that the GSM and OC3 algorithms are not suitable for Chl-*a* estimations over the Persian Gulf even in the deeper areas.

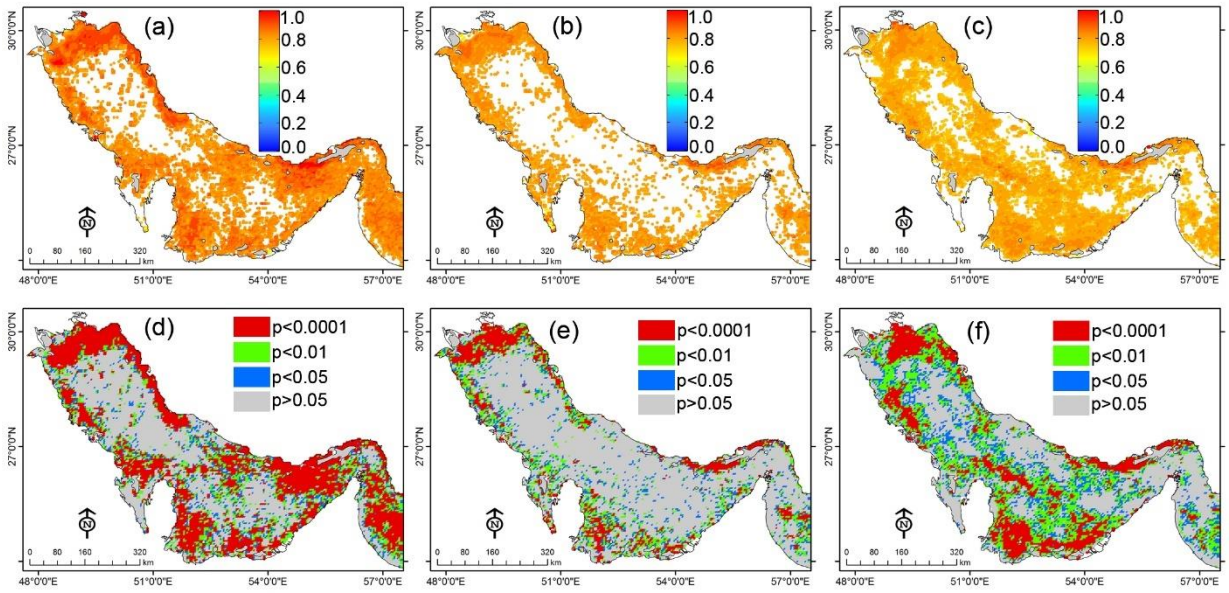

Figure 3. Maps of the correlation coefficient (r) between the monthly Chl-a time-series from MODIS using different Chl-a retrieval algorithms, Comparison-II. (a) MODIS-SG vs. MODIS-SI, (b) MODIS-SG vs. MODIS-SO, (c) MODIS-SO vs. MODIS-SI. (d)-(f) maps show the statistical significance (p) of the correlations of (a), (b), and (c), respectively.

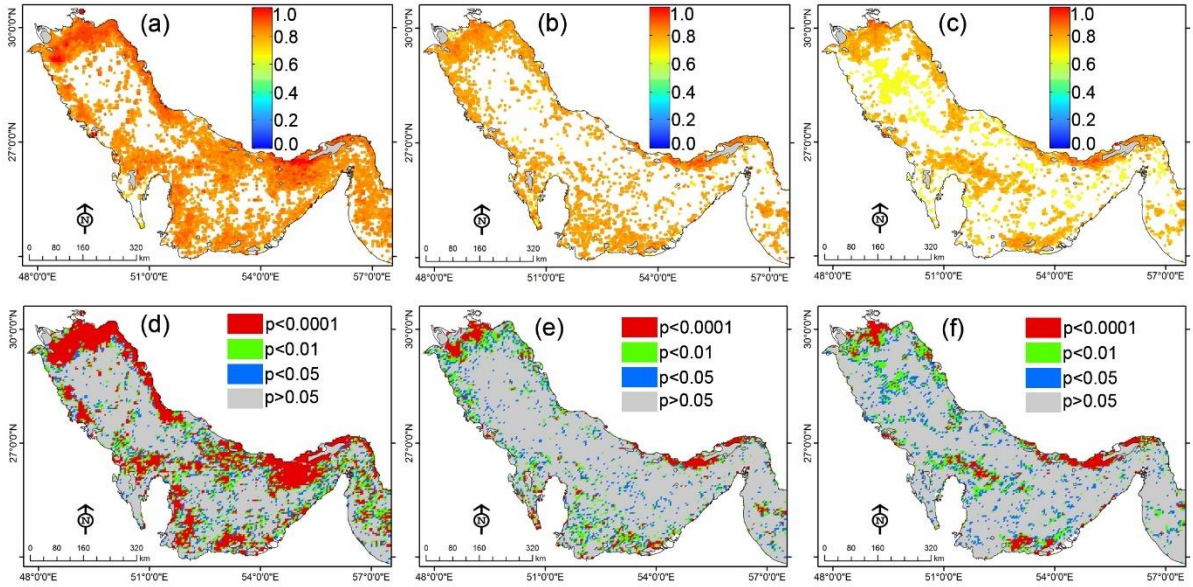

Figure 4. Maps of the correlation coefficient (r) between the monthly Chl-a anomalies from MODIS using different Chl-a retrieval algorithms, Comparison-II. (a) MODIS-SG vs. MODIS-SI, (b) MODIS-SG vs. MODIS-SO, (c) MODIS-SO vs. MODIS-SI. (d)-(f) maps show the statistical significance (p) of the correlations of (a), (b), and (c), respectively.

3.3. Comparison of different Chl-a retrieval algorithms from different sensors (Comparison-III)

Maps of the correlation coefficient (r) between monthly Chl-*a* time-series from different satellite sensors using different Chl-*a* retrieval algorithms are shown in Fig. 5. Only the results of Fig. 5b is consistent with Fig. 1, which indicates the correlations between MERIS-SO and SeaWiFS-SI are consistent with MERIS-SO and SeaWiFS-SO products. About 88% of the study area are significantly correlated for MERIS-SO vs. SeaWiFS-SI, and the other pairs of comparisons in *Comparison-III* scenario show less than 30% are significantly correlated over the shallow areas (Table 2). In addition, Fig. 4 indicates the influence of inter-sensor differences on the correlation maps and shows that the r-values and p-values between MERIS and SeaWiFS are higher than the other pairs over the whole Persian Gulf. Fig. 6 shows correlation coefficient maps between Chl-*a* anomalies from different satellite sensors using different Chl-*a* retrieval algorithms. It is consistent with Fig. 5 and indicates that the Chl-*a* anomalies between MERIS-SO and SeaWiFS-SI are significantly correlated for 67% of the whole study area (Fig. 6b, e).

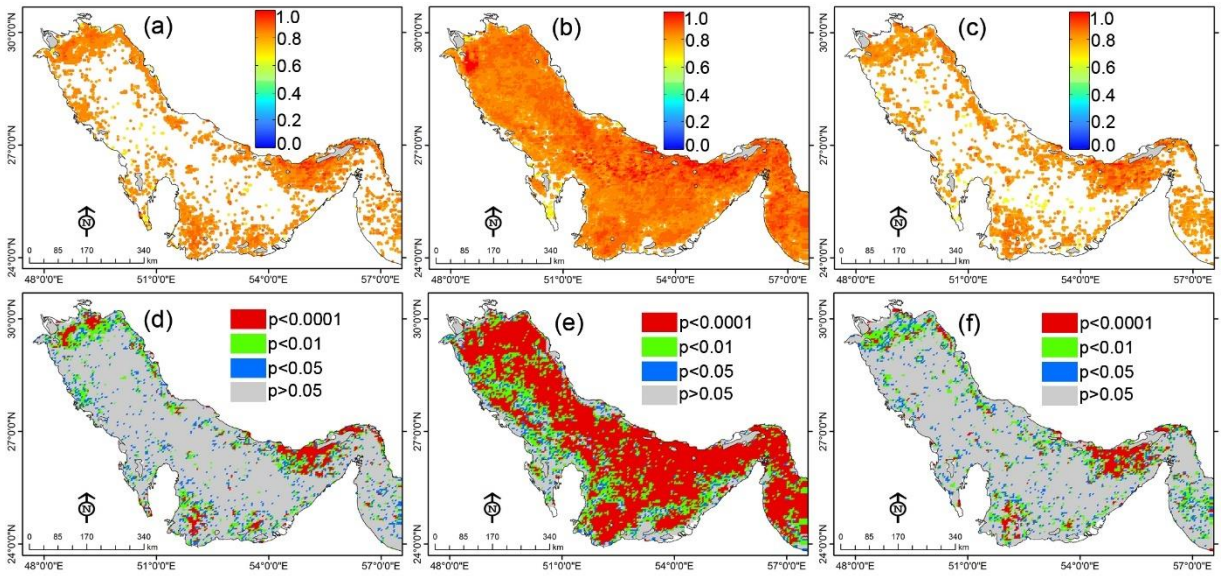

Figure 5. Maps of the correlation coefficient (r) between the monthly Chl-a time-series from different satellite sensors using different Chl-a retrieval algorithms, Comparison-III. (a) MERIS-SO vs. MODIS-SG, (b) MERIS-SO vs. SeaWiFS-SI, and (c) MODIS-SG vs. SeaWiFS-SI. (d)-(f) maps show the statistical significance (p) of the correlations of (a), (b), and (c), respectively.

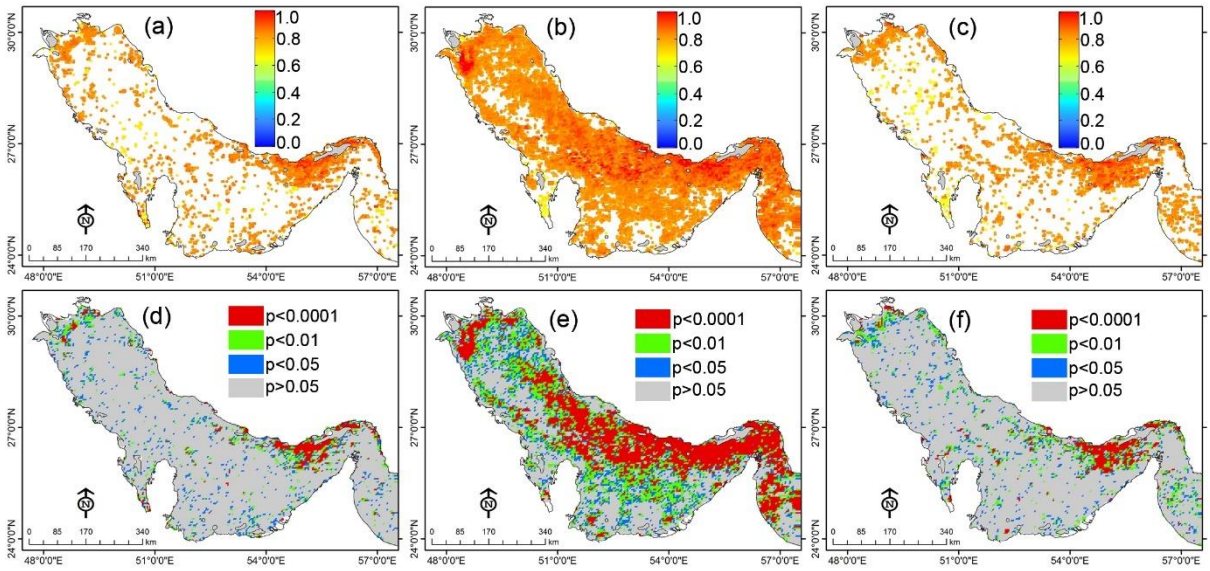

Figure 6. Maps of the correlation coefficient (r) between the monthly Chl-a anomalies from different satellite sensors using different Chl-a retrieval algorithms, Comparison-III. (a) MERIS-SO vs. MODIS-SG, (b) MERIS-SO vs. SeaWiFS-SI, and (c) MODIS-SG vs. SeaWiFS-SI. (d)-(f) maps show the statistical significance (p) of the correlations of (a), (b), and (c), respectively.

when compared with Chl-*a* retrieval algorithms from the same sensor (Fig. 3), the r-values are lower than for a single sensor, indicating the discrepancies of inter-sensor Chl-*a* estimations. However, the correlation coefficients for GSM and OC3/OC4 algorithms (<0.88) are less than the corresponding values of the OCI (>0.9) algorithm. Nonetheless, correlation maps of the *Comparison-III* scenario indicate the consistency in the Chl-*a* time-series and anomalies irrespective of the choice in Chl-*a* retrieval algorithms, although the most of the study area (75-84%) for GSM and OC3/OC4 algorithms are not significantly correlated.

3.4. Comparison of different atmospheric correction algorithms (Comparison-IV)

The maps of the correlation coefficient (r) between the monthly Chl-*a* time-series from different satellite sensors (MERIS, MODIS, and SeaWiFS) using two different atmospheric correction algorithms (SeaDAS and POLYMER) are shown in Fig. 7. The Chl-*a* time-series are significantly for 21-26% of the whole study area (Table 2), and most of the study area (74-79%) show insignificant correlations. However, the r-values from different satellite sensors in *Comparison-IV* varies from 0.82-0.97 (Fig. 7a-c). Fig. 8 shows maps of the correlation coefficient (r) between monthly Chl-*a*

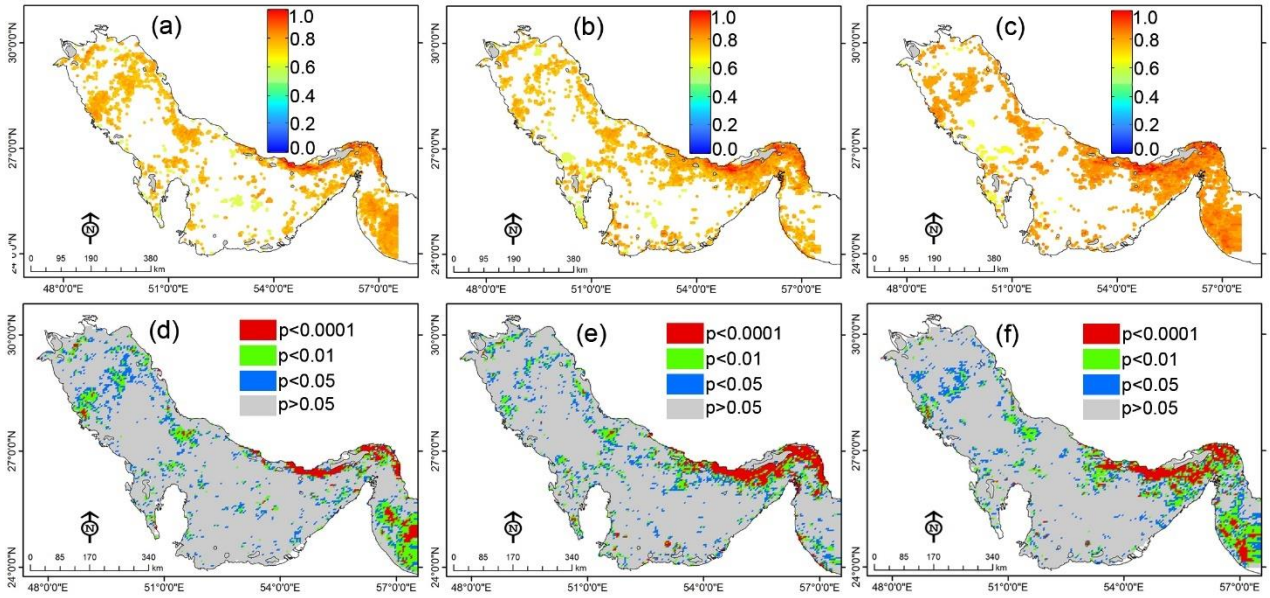

Figure 7. Maps of the correlation coefficient (r) between the monthly Chl-a time-series from different satellite sensors using different atmospheric correction algorithms, Comparison-IV. (a) MODIS-SO vs. MMERIS-PO, (b) MERIS-SO vs. MERIS-PO, and (c) SeaWiFS-SO vs. MERIS-PO. (d)-(f) maps show the statistical significance (p) of the correlations of (a), (b), and (c), respectively.

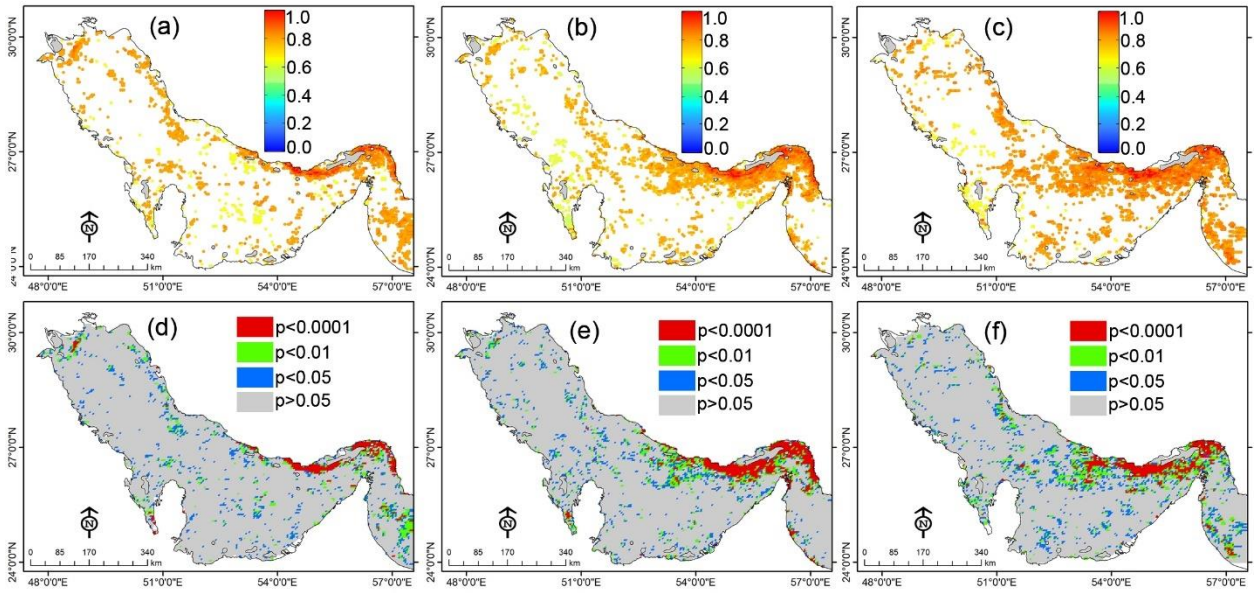

Figure 8. Maps of the correlation coefficient (r) between the monthly Chl-a anomalies from different satellite sensors using different atmospheric correction algorithms, Comparison-IV. (a) MODIS-SO vs. MMERIS-PO, (b) MERIS-SO vs. MERIS-PO, and (c) SeaWiFS-SO vs. MERIS-PO. (d)-(f) maps show the statistical significance (p) of the correlations of (a), (b), and (c), respectively.

anomalies for the pairs of *Comparison-IV* scenario where 79-87% of the study area show imperfect correlations (Table 2). Results are consistent with those obtained between GSM and OC3/OC4 Chl-*a* retrieval algorithms (Fig. 5, 6).

Results of the comparison between MODIS-SO and MERIS-PO, and the comparison between SeaWiFS-SO and MERIS-PO show the effect of both different atmospheric correction algorithms and different sensors, whereas comparison between MERIS-PO and MERIS-SO are just influenced by different atmospheric correction algorithms. The correlations between MERIS-PO and MERIS-SO are generally greater in northern coastal regions and they are slightly lower in the middle and southern regions (<0.74). In general, results of the Comparison-IV scenario (Fig. 7 and 8) indicate that the consistency of the Chl-*a* time-series and anomalies between different satellite sensors irrespective of the choice of atmospheric correction algorithms are imperfect over more than 70% of the Persian Gulf. Therefore, it could be concluded that the SeaDAS and POLYMER algorithms are not significantly correlated over the Persian Gulf.

4. Discussion

The Chl-*a* time-series for SeaWiFS, MERIS, and MODIS, are significantly correlated for >84% of the whole Persian Gulf (Table 2). Also, it was found that MODIS and VIIRS are correlated (~0.9) over the 37% of the study area, and the reminders are imperfectly correlated (Fig. 1). Furthermore, correlations between anomalies of the Chl-*a* from different satellite sensors are consistent with those obtained form Chl-*a* time series, although the spatial extent of prefect correlations are lower than Chl-*a* time-series (Fig. 2). It is encouraging to see such consistency in the Chl-a datasets from different satellite sensors despite of differences in design, wavelengths, overpass time, and pre- and post-lunch calibration instrument characteristics of each sensor. An irregular temporal sampling of ocean color satellite sensors produces biases in the monthly Chl-*a* series which is observable in the regional interannual variabilities. In addition, missing data and gaps in ocean color datasets may increase the inconsistency between different satellite sensors. The correlation between Chl-*a* from different satellite sensors appears reasonably sensitive to the Chl-*a* retrieval algorithms (Fig. 4-6), and to the atmospheric correction algorithms (Fig. 7 and 8). In this regard, SeaDAS and POLYMER atmospheric correction algorithms are highly consistent and no more significant differences were observed. In contrast, OC3/OC4 and OCI of Chl-*a* retrieval algorithms show very different results over the study area, where OCI showed more consistent results than OC3/OC4 algorithms for all of the selected satellite sensors. The analysis of the Chl-*a* anomalies showed similar results. The interannual consistency between different satellite sensors shows that the biases between sensors and algorithms are minimized. Also, it confirms the high stability and sensor calibration of the selected ocean color sensors.

It is clear from different satellite sensors that the differences of Chl-*a* raised mainly from different Chl-a retrieval algorithms (OC3/OC4, GSM, and OCI). However, along the middle and southern coastal regions, higher differences in Chl-*a* are observed when applying different atmospheric correction algorithms compared with different Chl-*a* retrieval algorithms. This finding indicates that the accurate atmospheric correction is clearly affects the Chl-*a* estimations from ocean color satellite sensors. Over the southern and middle of the Persian Gulf dust deposition and aerosol content raised from adjacent Sahara significantly influence the Chl-*a* estimation and emphasizes on the selection of an accurate atmospheric correction algorithm. Choosing the best atmospheric correction algorithm between POLYMER and SeaDAS for SeaWiFS, MERIS, and MODIS over the study area requires more investigation which is beyond the scope of this study.

Most of the ocean color satellites have life cycles of 5-10 years, and many of them have completed their mission (e.g. MERIS and SeaWiFS). Long-term detection of seasonal and interannual variations of Chl-*a* requires the combination of different ocean color missions which have overlapped to enable cross-calibration. The SeaWiFS, MERIS, and MODIS sensors have operated in parallel for 8 years, and MODIS and VIIRS are in orbit from 9 years ago. Hence, the results of this study provide an insight for merging of the selected satellite sensors for long-term analysis of Chl-*a*.

5. Conclusion

In this study, we used the monthly Chl-*a* time-series during the last 20-year period to evaluate the temporal consistency between four satellite sensors, SeaWiFS, MERIS, MODIS, and MODIS. Monthly anomalies of the Chl-*a* series were calculated for each satellite sensor over the study time period. Statistical analysis revealed that the Chl-*a* time-series and anomalies of three sensors were correlated for >84% and 63% of the study area, respectively. Chl-a series and anomalies from VIIRS showed to be correlated with MODIS over 37% and 34% of the study area. The consistency between different atmospheric correction and Chl-*a* retrieval algorithms from different sensors revealed that the accurate selection of Chl-*a* retrieval and atmospheric correction algorithms are very critical over the study area. The Chl-*a* time-series and anomalies showed consistency between GSM and OCI Chl-*a* retrieval algorithms in shallow regions where Chl-*a* concentrations are >0.3 mg m^{-3}. The OC3M and OC4 algorithms showed the lowest correlation with GSM algorithm in both shallow and deep regions of the Persian Gulf. The results indicated that the OC3/OC4 and GSM algorithms are not suitable for Chl-*a* estimations over the whole area of the study area, and in contrast the OCI algorithm provides more reasonable estimations of Chl-*a*. Furthermore, results revealed that the different atmospheric correction algorithms are reasonably influence the Chl-*a* estimations from different satellite sensors. In this regard, more than 70% of the study area showed an imperfect consistency between SeaDAS and POLYMER atmospheric correction algorithms. Consequently, performing the best atmospheric correction, and Chl-*a* retrieval algorithms are critical tasks in Chl-*a* estimations and applications in the Persian Gulf. The results also provide a decision for combining the ocean color satellite products for performing the long-term Chl-*a* datasets, while properly minimize the systematic differences between different satellite sensors.

Acknowledgment

This work has been supported by the Center for International Scientific Studies & Collaboration (CISSC), ministry of Science Research and

Technology. I express my gratitude to Dr. Masoud Sadreenasab, president of CISSC, for his kind cooperation.

6. References

[1] Saba VS, Friedrichs MAM, Antoine D, Armstrong RA, Asanuma I, Behrenfeld MJ, et al. (2011). An evaluation of ocean color model estimates of marine primary productivity in coastal and pelagic regions across the globe. *Biogeosciences*. 8(2):489–503.

[2] Gregg WW, Rousseaux CS. (2014). Decadal trends in global pelagic ocean chlorophyll: A new assessment integrating multiple satellites, in situ data, and models. *Journal of Geophysical Research C: Oceans*.119(9):5921–33.

[3] Brewin RJW, Sathyendranath S, Müller D, Brockmann C, Deschamps PY, Devred E, et al. (2015). The Ocean Colour Climate Change Initiative: III. A round-robin comparison on in-water bio-optical algorithms. *Remote Sensing of Environment*.162.

[4] Brickley PJ, Thomas AC. (2004). Satellite-measured seasonal and inter-annual chlorophyll variability in the Northeast Pacific and Coastal Gulf of Alaska. *Deep-Sea Research Part II: Topical Studies in Oceanography*.51(1–3):229–45.

[5] Kim W, Moon JE, Park Y, Ishizaka J. (2016). Evaluation of chlorophyll retrievals from Geostationary Ocean Color Imager (GOCI) for the North-East Asian region. *Remote Sensing of Environment*. 184:482–95.

[6] Song H, Long MC, Gaube P, Frenger I, Marshall J, McGillicuddy DJ. (2018). Seasonal Variation in the Correlation Between Anomalies of Sea Level and Chlorophyll in the Antarctic Circumpolar Current. *Geophysical Research Letters*. 45(10):5011–9.

[7] Mannino A, Novak MG, Nelson NB, Belz M, Berthon J-F, Blough N V., et al. (2019). Measurement protocol of absorption by chromophoric dissolved organic matter (CDOM) and other dissolved materials. IOCCG Ocean Optics and Biogeochemistry Protocols for Satellite Ocean Colour Sensor Validation. 1:1–77.

[8] Blauw AN, Benincà E, Laane RWPM, Greenwood N, Huisman J. (2018). Predictability and environmental drivers of chlorophyll fluctuations vary across different time scales and regions of the North Sea. *Progress in Oceanography*. 161:1–18.

[9] Sathyendranath S, Brewin RJ, Brockmann C, Brotas V, Calton B, Chuprin A, et al. (2019). An ocean-colour time series for use in climate studies: The experience of the ocean-colour climate change initiative (OC-CCI). *Sensors*. 19(19):4285.

[10] Allison DB, Stramski D, Mitchell BG. (2010). Seasonal and interannual variability of particulate organic carbon within the Southern Ocean from satellite ocean color observations. *Journal of Geophysical Research: Oceans*. 115(6).

[11] IOCCG. (2014). Phytoplankton functional types from Space. *Reports and Monographs of the International OceanColour Coordinating Group*. (15).

[12] Westberry TK, Schultz P, Behrenfeld MJ, Dunne JP, Hiscock MR, Maritorena S, et al. (2016). Annual cycles of phytoplankton biomass in the subarctic Atlantic and Pacific Ocean. *Global Biogeochemical Cycles*. 30(2):175–90.

[13] Friedland KD, Mouw CB, Asch RG, Ferreira ASA, Henson S, Hyde KJW, et al. (2018). Phenology and time series trends of the dominant seasonal phytoplankton bloom across global scales. *Global Ecology and Biogeography*. 1;27(5):551–69.

[14] Shang SL, Dong Q, Hu CM, Lin G, Li YH, Shang SP. (2014). On the consistency of MODIS chlorophyll-a products in the northern South China Sea. *Biogeosciences*. 11(2):269–80.

[15] Al-Naimi N, Raitsos DE, Ben-Hamadou R, Soliman Y. (2017). Evaluation of satellite retrievals of chlorophyll-a in the Arabian Gulf. *Remote Sensing*. 2017; 9(3).

[16] Moradi M, Kabiri K. (2015). Spatio-temporal variability of SST and Chlorophyll-a from MODIS data in the Persian Gulf. *Marine Pollution Bulletin*. 98(1–2):14–25.

[17] Swift SA, Bower AS. (2003). Formation and circulation of dense water in the Persian/Arabian Gulf. *Journal of Geophysical Research: Oceans*. 108(1).

[18] Vaughan GO, Al-Mansoori N, Burt JA. (2018). The arabian gulf. In: World Seas: An Environmental Evaluation Volume II: The Indian Ocean to the Pacific., 1–23.

[19] Paparella F, Xu C, Vaughan GO, Burt JA. (2019). Coral bleaching in the Persian/Arabian Gulf is modulated by summer winds. *Frontiers in Marine Science*. 6(1).

[20] Al-Yamani F, Naqvi SWA. (2019). Chemical oceanography of the Arabian Gulf. *Deep-Sea Research Part II: Topical Studies in Oceanography*. 161:72–80.

[21] Hunter JR. (1983). Aspects of the dynamics of the residual circulation of the Arabian Gulf. *Coastal Oceanography*. 31–42.

[22] Nezlin NP, Polikarpov IG, Al-Yamani F. (2007). Satellite-measured chlorophyll distribution in the Arabian Gulf: Spatial, seasonal and inter-annual variability. *International Journal of Oceans and Oceanography*. 2(1):139–56.

[23] Nezlin NP, Polikarpov IG, Al-Yamani FY, Subba Rao D V., Ignatov AM. (2010). Satellite monitoring of climatic factors regulating phytoplankton variability in the Arabian (Persian) Gulf. *Journal of Marine Systems*. 82(1–2):47–60.

[24] Ghanea M, Moradi M, Kabiri K. (2015). Investigation the behavior of MODIS ocean color products under the 2008 red tide in the eastern

Persian Gulf. In: International Archives of the Photogrammetry, *Remote Sensing and Spatial Information Sciences - ISPRS Archives*. p. 227–32.

[25] Fallahi, M., Torabi Azad, M., & Mansoury, D. (2021). A Hydrodynamic Model of Tidal Current in the Strait of Hormuz. *International Journal of Coastal and Offshore Engineering*, 5(1), 37-45.

[26] Moradi M, Moradi N. (2020). Correlation between concentrations of chlorophyll-a and satellite derived climatic factors in the Persian Gulf. *Marine Pollution Bulletin*. 161.

[27] Moradi, M. (2022). Inter-comparison of single-sensor and merged multi-sensor ocean color chlorophyll-a products in the shallow turbid waters-case study: Persian Gulf. *International Journal of Coastal and Offshore Engineering*, 7(2), 1-10.

[28] Werdell PJ, Franz BA, Bailey SW, Harding, Jr. LW, Feldman GC. (2007). Approach for the long-term spatial and temporal evaluation of ocean color satellite data products in a coastal environment. In: *Coastal Ocean Remote Sensing*. p. 66800G.

[29] Bailey SW, Werdell PJ. (2006). A multi-sensor approach for the on-orbit validation of ocean color satellite data products. *Remote Sensing of Environment*. 102(1–2):12–23.

[30] Hu C, Feng L, Lee Z. (2013). Uncertainties of SeaWiFS and MODIS remote sensing reflectance: Implications from clear water measurements. *Remote Sensing of Environment*. 133:168–82.

[31] Uitz J, Claustre H, Gentili B, Stramski D. (2010). Phytoplankton class-specific primary production in the world's oceans: Seasonal and interannual variability from satellite observations. *Global Biogeochemical Cycles*. 24(3).

[32] Vantrepotte V, Loisel H, Mlin F, Desailly D, Duforêt-Gaurier L. (2011). Global particulate matter pool temporal variability over the SeaWiFS period (1997-2007). *Geophysical Research Letters*. 38(2).

[33] Loisel H, Vantrepotte V, Ouillon S, Ngoc DD, Herrmann M, Tran V, et al. (2017). Assessment and analysis of the chlorophyll-a concentration variability over the Vietnamese coastal waters from the MERIS ocean color sensor (2002–2012). *Remote Sensing of Environment*. 190:217–32.

[34] Cui T, Zhang J, Tang J, Sathyendranath S, Groom S, Ma Y, et al. (2021). Assessment of satellite ocean color products of MERIS, MODIS and SeaWiFS along the East China Coast (in the Yellow Sea and East China Sea). *ISPRS Journal of Photogrammetry and Remote Sensing*. 87:137–51.

[35] Yu Z, Yang K, Luo Y, Shang C. (2020). Spatial-temporal process simulation and prediction of chlorophyll-a concentration in Dianchi Lake based on wavelet analysis and long-short term memory network. *Journal of Hydrology*. 582.

[36] Le C, Hu C, Cannizzaro J, Duan H. (2013). Long-term distribution patterns of remotely sensed water quality parameters in Chesapeake Bay. *Estuarine, Coastal and Shelf Science*. 128:93–103.

[37] Campbell JW. (1995). The lognormal distribution as a model for bio-optical variability in the sea. *Journal of Geophysical Research*. 100(C7).

[38] Greene CA, Thirumalai K, Kearney KA, Delgado JM, Schwanghart W, Wolfenbarger NS, et al. (2019). The Climate Data Toolbox for MATLAB. Geochemistry, Geophysics, *Geosystems*. 20(7):3774–81.

[39] Siegel DA, Behrenfeld MJ, Maritorena S, McClain CR, Antoine D, Bailey SW, et al. (2013). Regional to global assessments of phytoplankton dynamics from the SeaWiFS mission. *Remote Sensing of Environment*. 135:77–91.

[40] Cohen P, Cohen P, West SG, Aiken LS. (2014). Applied Multiple Regression/Correlation Analysis for the Behavioral Sciences. Applied Multiple Regression/Correlation Analysis for the Behavioral Sciences. *Psychology Press*.